Proceedings of the 7th International Young Geotechnical Engineers Conference – Scott (Ed.)

Seismic behaviour of structures with basements in liquefiable soil

Comportement sismique des structures avec des sous-sols dans un sol liquéfiable

Fiona Hughes
Geotechnics, Arup, UK, fiona.hughes@arup.com

Gopal Madabhushi
Department of Engineering, University of Cambridge, UK

ABSTRACT: The inclusion of basements can provide uplift forces during the liquefied period thereby reducing overall settlement of structures. This phenomenon has been investigated using dynamic geotechnical centrifuge modelling at the University of Cambridge, where the effect of the presence of a basement structure on a single degree of freedom building sited on liquefiable soil has been investigated. In this paper, the dynamic response of the structure during three shaking events is presented. When positive excess pore pressures are generated during earthquake induced liquefaction, the uplift force provided by a basement increases above that in hydrostatic conditions. Consequently, the effective weight of the structure reduces. This has been found to have the positive effect of reducing liquefaction induced settlement of the structure, compared to structures with shallow foundations without basement. In addition, generation of excess pore pressure, and the reduction in effective vertical stress that ensues, result in the stiffness of the soil approaching an almost zero value. Transmission of S_h waves therefore decrease, causing horizontal accelerations to be attenuated as they are transmitted upwards from the base of the model, resulting in natural isolation of the structure.

RÉSUMÉ : L'inclusion de sous-sols peut fournir des forces de soulèvement pendant la période de liquéfaction, réduisant ainsi le tassement global des structures. Ce phénomène a été étudié à l'aide d'une modélisation géotechnique dynamique par centrifugation à l'Université de Cambridge, où l'effet de la présence d'une structure de socle sur un bâtiment à un seul degré de liberté situé sur un sol liquéfiable a été étudié. Dans cet article, la réponse dynamique de la structure au cours de trois événements de secousses est présentée. Lorsque des surpressions interstitielles positives sont générées pendant la liquéfaction induite par un tremblement de terre, la force de soulèvement fournie par un sous-sol augmente au-dessus de celle dans des conditions hydrostatiques. Par conséquent, le poids effectif de la structure diminue. Cela s'est avéré avoir l'effet positif de réduire le tassement des structures induit par la liquéfaction, par rapport aux structures avec des fondations peu profondes sans sous-sol. De plus, la génération d'une surpression interstitielle et la réduction de la contrainte verticale effective qui s'ensuit entraînent une rigidité du sol proche d'une valeur presque nulle. La transmission des ondes Sh diminue donc, entraînant une atténuation des accélérations horizontales au fur et à mesure qu'elles sont transmises vers le haut depuis la base du modèle, entraînant un isolement naturel de la structure.

KEYWORDS: liquefaction, basement, settlement, isolation, centrifuge.

1 INTRODUCTION

Earthquake induced liquefaction is continuing to cause significant damage in the built environment. On level ground, this is primarily due to its effect on structures with shallow foundations, which have been repeatedly observed to experience rotation and large settlement (Cubrinovski et al. 2011, Yasuda et al. 2012, Bertalot et al. 2013). Significant research has been conducted to investigate the effect of a number of parameters on this failure type, including the depth of the liquefiable layer, structure bearing pressure, width of the structure, and shaking intensity, to name a few (Dashti et al. 2010a, Bertalot & Brennan 2015, Adamidis & Madabhushi 2018). Another highly researched problem caused by liquefaction in the built environment is the uplift of subsurface structures which have a unit weight lower than the liquefied soil surrounding them - for example pipelines, empty storage tanks or underground car parks (Koseki et al. 1997, Yang et al. 2004, Chian and Madabhushi 2012).

The behaviour of structures partially buried in liquefiable ground, which is the case for many modern buildings with basements, is not well understood. Intuitively, buildings of this nature combine the propensity of surface structures to settle and light subsurface structures to float, and therefore may result in a reduced total vertical displacement. The aim of this paper is to look at the soil-structure interaction for a structure with a basement during earthquake induced liquefaction.

2 METHODOLOGY

A series of dynamic centrifuge experiments have been undertaken using the 10 m diameter Turner beam centrifuge at the Schofield Centre at the University of Cambridge (Schofield, 1980). Results from one of these tests will be presented and discussed here.

The test presented here was conducted in a rigid container with a Perspex window which allows digital image correlation to be conducted. Plane strain conditions were replicated. A layer of Duxseal at both ends of the container limited the effect of the rigid boundaries (Steedman and Madabhushi, 1991). A homogenous layer of loose Hostun HN31 sand was poured by air pluviation using an automatic sand pourer (Chian, Stringer and Madabhushi, 2010). Properties of the Hostun sand used are as follows: G_s=2.65, d_{50}=0.424 mm, e_{min}=0.555, e_{max}=1.01 and ϕ_{crit}=33 ° (Mitrani, 2006). The target relative density was 44%, equating to a saturated unit weight of 18.8 kNm^{-3}. Arrays of instruments were placed underneath the structure and in the far-field. Piezoelectric accelerometers, linear variable differential transformers (LVDTs), micro mechanical system accelerometers (MEMS), and pore pressure transducers (PPTs) were used. The locations of the instruments discussed in this paper are shown in Figure 1.

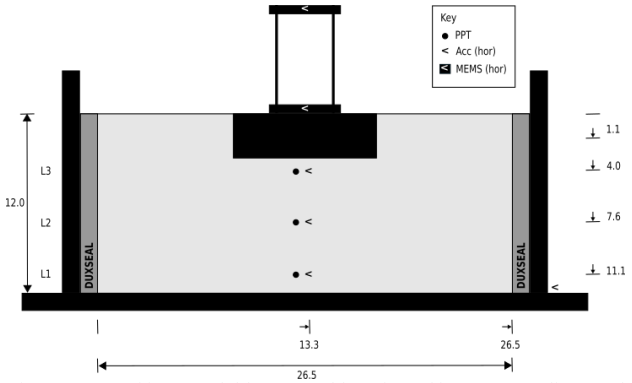

Figure 1. Centrifuge model layout and location of instruments discussed in this paper. Dimensions in m, prototype scale.

The test was conducted at a centrifugal acceleration of 60 g. The model was saturated with a high viscosity aqueous solution of hydroxypropyl methylcellulose with a viscosity of 60 cSt. This was done using CAM-Sat, an automated, pressure-controlled system (Stringer and Madabhushi, 2010).

2.1 *Vertical forces*

The basement of the structure was designed to provide an uplift force equal to a specified percentage of the total weight of the structure when the surrounding soil fully liquefied, with the aim to prevent the structure from settling. This design philosophy is similar to that of "floating" or "compensated" foundations used to reduce structure settlement in locations with soft soil conditions, and can also be likened to the design of boats.

Vertical forces acting on the structure in static conditions and in the event of complete soil liquefaction are shown in Figure 2. In static conditions, an upward buoyancy force is present ($F_{U,H}$) due to the hydrostatic water pressure (u_{hy}). The upward buoyancy force can be calculated using Eq. 1:

$$F_{U,H} = u_{hy} \times A = \gamma_w d \times A = \gamma_w \times V \quad (1)$$

where V, A and d are the volume, cross sectional area and depth of the basement respectively and γ_w is the unit weight of water. This uplift force is resisted by the weight of the superstructure and basement (F_S and F_B respectively) and the shear resistance along the soil-structure interface (F_F), as shown in Figure 2a. A resultant vertical force acts vertically downwards, which results in the effective bearing pressure given in Table 1.

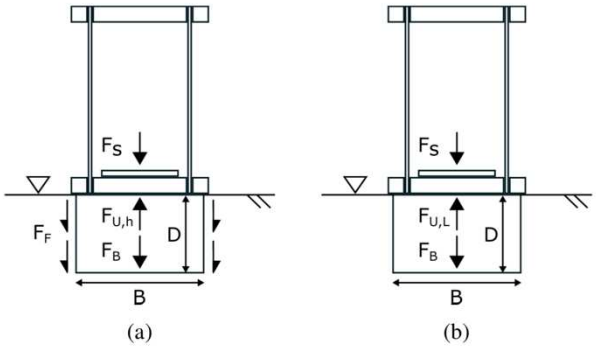

Figure 2. Vertical forces acting on a structure with a basement (a) static conditions, (b) in the event of liquefaction. Forces are shown by single-headed arrows. Dimensions are shown by double-headed arrows.

In the event of complete soil liquefaction, the shear resistance of the soil reduces significantly so the shear resistance along the soil-structure interface is assumed to be negligible (Koseki et al. 1997). In addition, the uplift force acting on the structure ($F_{U,L}$) increases to greater than the hydrostatic value ($F_{U,H}$). This can be considered in two ways, as shown in Eq. 2, 3, and 4. Firstly, excess pore pressures (u_{ex}) are generated and act on the bottom of the basement in addition to the hydrostatic pressure present in the static analysis:

$$F_{U,L} = F_{U,H} + u_{ex} \times A \quad (2)$$

When full liquefaction occurs, the excess pore pressure generated becomes equal to the initial vertical effective stress in the soil, and Eq. 2 becomes:

$$F_{U,L} = F_{U,H} + \gamma'_s d \times A = (\gamma_w + \gamma'_s) \times V = \gamma_s V \quad (3)$$

where γ_s and γ'_s are the saturated and buoyant unit weight of the soil respectively.

Alternatively, the total uplift force can be calculated using Archimedes' principle, assuming the soil behaves as a dense fluid when liquefied. Archimedes' principle states that any body completely or partially submerged in a fluid at rest is acted upon by an upward, buoyant force, the magnitude of which is equal to the weight of the fluid displaced by the body:

$$F_{U,L} = \gamma_s V \quad (4)$$

Equations 3 and 4 show that these methods are equivalent when liquefaction occurs and the excess pore pressure generated is equal in magnitude to the initial vertical effective stress in the soil. The ratio of the uplift, U, to total weight, W, when the surrounding soil liquefies (see Eq. 5) was used as a design parameter for the structures tested in this research:

$$U/W = F_{U,L}/(F_S + F_B) \quad (5)$$

2.2 *Model structure*

The model structure used in this centrifuge test consisted of a single degree of freedom (SDOF) sway frame rigidly connected to a rigid basement structure which was constructed out of sheet aluminium surrounding closed-cell foam. Structural properties, in prototype scale, are given in Table 1.

Table 1. Properties of structure (prototype scale)

Property	
Total bearing pressure (kPa)	55.0
Effective bearing pressure (kPa)	29.0
Superstructure height (m)	7.2
Basement width (m)	9.6
Basement depth (m)	3.0
CoG height above top of basement (m)	0.53
Fixed base natural frequency (Hz)	1

2.3 *Base shaking*

A servo- hydraulic earthquake actuator was used to generate one dimensional input motions (Madabhushi et al., 2012). The base shaking of the events discussed in this paper had the characteristics listed in Table 2. In this table the last column shows the time duration between dissipation of 5 % and 95 % of the total Arias intensity (Arias, 1970).

Table 2. Base shaking characteristics (prototype scale).

	EQ1	*EQ2*	*EQ3*
Waveform	Sinusoidal	Imperial Valley	Sinusoidal
Freq (Hz)	1	-	1
Peak acc (g)	0.035	0.131	0.424
$T_{5\text{-}95}$ (s)	17.4	28.7	17.8

3 DYNAMIC BEHAVIOUR OF BASEMENT-STRUCTURE SYSTEM

3.1 *Generation of excess pore pressures*

The base shaking of the events discussed in this paper had different duration, peak acceleration, and frequency content, shown in Table 2. The first earthquake (EQ1) had a low amplitude, sinusoidal input motion. The second earthquake (EQ2) had the same frequency content as the 1979 Imperial Valley earthquake, which is characterised by its long duration and high frequency content. The third earthquake (EQ3) was a high amplitude, sinusoidal input motion with the same number of cycles and the same frequency as EQ1. Consequently, the excess pore pressures generated in each event varied greatly.

Soil densification occurred as a result of each of the shaking events therefore the soil relative density prior to each earthquake event varied slightly. The relative densities were calculated using the mass of sand in the container and the volume occupied before each shaking event commenced, and were 49 %, 49 % and 53 %, before EQ1, EQ2 and EQ3 respectively. Post EQ3 the relative density increased to 63 %. The pre-seismic soil condition remained susceptible to liquefaction prior to each earthquake therefore it is assumed that the soil behaviour during each of seismic events can be compared. Figure 3 shows the excess pore water pressures generated in the instrumented column of soil beneath the centre of the basement.

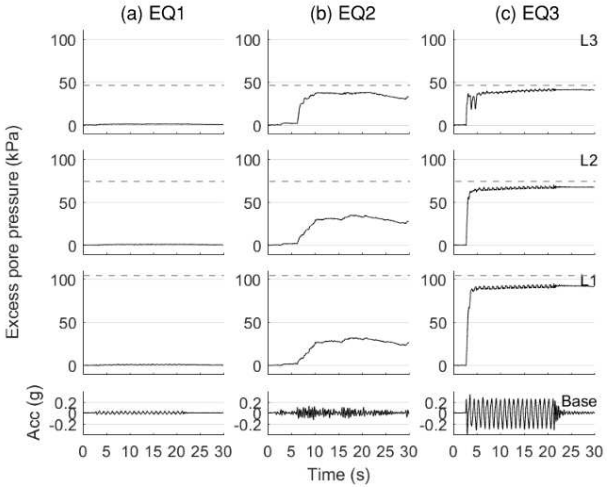

Figure 3. Excess pore pressures generated in the soil column beneath the structure during (a) EQ1, (b) EQ2, and (c) EQ3. Dashed lines indicate the initial vertical effective stress at the corresponding location obtained from Plaxis 2D analysis.

The low amplitude of the base shaking of EQ1was not sufficient to cause contraction of the loose soil skeleton, resulting in no excess pore pressure generation in the soil beneath the structure (Figure 3a). The only difference between the base shaking in EQ1 and EQ3 was the amplitude of the base shaking; the base shaking consisted of 20 cycles of sinusoidal motion with a frequency of 1 Hz prototype scale. In EQ3 excess pore pressures were generated at all depths below the structure (Figure 3c). The excess pore pressures generated increased with increasing depth, due to the capacity for excess pore pressure generation increasing with depth due to a greater initial vertical stress (total and effective). Most previous investigations into earthquake induced liquefaction soil-structure interaction have used structures with a significantly greater bearing pressure than that applied by the structure in this test, which has prevented full liquefaction occurring beneath the structure (Dashti et al., 2010b, Zeybek and Madabhushi, 2016, Adamidis and Madabhushi, 2018). The presence of the basement in the test presented in this paper significantly reduced the bearing pressure applied by the structure, to a level below that preventing full liquefaction from occurring. In static conditions the bearing pressure applied by the structure is reduced due to the hydrostatic pressure acting on the structure due to the basement being located below the water table. When liquefaction of the soil adjacent to the structure occurs, the uplift force acting on the structure increases further, leading to an additional reduction of the bearing pressure. When full liquefaction occurred to the depth of, or deeper than, the bottom of the basement the bearing pressure applied by the structure reduced to 2.9 kPa.

In EQ2, excess pore pressures were generated at all depths, with the rate of generation decreasing with increasing depth below the structure (Figure 3b). The excess pore pressures generated at the three instrumented depths were of roughly the same value during the co-seismic period. Full liquefaction therefore only occurred at the shallowest instrumented depth below the structure. At deeper depths, soil softening is anticipated to have occurred, proportional to the excess pore pressures generated, despite full liquefaction not occurring.

3.2 *Transmission of horizontal accelerations*

Horizontal accelerations were measured at discrete locations in the soil body and on the structures, as shown in Figure 1. Figure 4 shows the horizontal acceleration time histories for the roof and ground floor of the structures and the column of soil below the centre of the basements. In EQ1, excess pore pressures were not generated (Figure 3a). There was no attenuation of horizontal accelerations transmitted in the soil body beneath the structure (Figure 4a). The amplitude of the shaking of the ground floor of the structure was of the same magnitude as the base shaking. The flexible nature of the structure, which has a fixed base natural frequency equal to the frequency of the base shaking, resulted in the accelerations at the roof level being greater than those experienced at the ground floor level. The accelerations experienced at roof level were therefore of greater magnitude than the base shaking. Amplification is most significant for the first 7 cycles, reaching a maximum amplification factor equal to 2.7. Shaking of the structure ceased when base shaking ended.

In EQ2, the amplitude of the horizontal accelerations measured in the soil beneath the structure are the same as the base shaking (Figure 4b). The accelerations transmitted to the ground floor of the structure are attenuated as the soil adjacent to the structure liquefied. The embedment of the structure, provided by the rigid basement, means the horizontal accelerations transmitted to the structure are governed primarily by soil behaviour adjacent to the structure, rather than beneath it. Acceleration of the roof of the structure was attenuated compared to the base shaking.

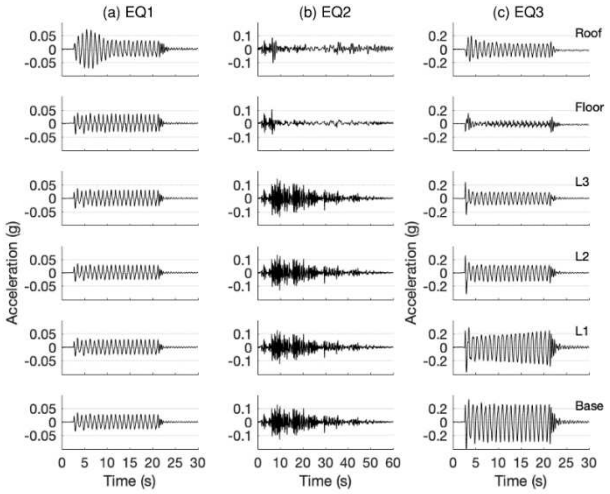

Figure 4. Co-seismic horizontal acceleration time histories for the structure, the soil column below the basement and the input motion during (a) EQ1, (b) EQ2, and (c) EQ3.

In EQ3 full liquefaction occurred at all instrumented depths beneath the structure (Figure 3c). Horizontal accelerations were progressively attenuated as they were transmitted upwards from the base of the model by S_h waves (Figure 4c). The horizontal accelerations transmitted to the structure were therefore significantly smaller than those generated by the base shaking. Generation of excess pore pressure, and the reduction in effective vertical stress that ensues, result in the stiffness of the soil approaching an almost zero value. Transmission of S_h waves therefore decrease, causing horizontal accelerations to be attenuated. Horizontal accelerations transmitted to the ground floor of the structure were then amplified at the roof level since they were close to the fixed base natural frequency of the structure. In contrast to EQ1, in EQ3 the accelerations at roof level were less than the base shaking. The maximum amplification factor was 0.81 which occurred during the second cycle of shaking, before reducing to approximately 0.5 from the fifth cycle onwards. This is due to attenuation within the liquefied soil layer. Shaking of the structure ceased when the base shaking ended.

3.3 *Stress paths*

The stress paths at the depth of L2 of instrumentation, 7.1 m below the soil surface, which corresponds to 4.1 m below the bottom of the basement, are presented in Figure 5 for the three earthquakes. The critical state line, CSL, is shown by the thin grey line. Vertical effective stress was calculated by subtracting the measured excess pore pressure from the corresponding initial vertical effective stress obtained from Plaxis 2D analysis. Shear stress was calculated using acceleration data, following the methodology proposed by Elgamal et al. (1996).

During EQ1 and EQ2, the stress paths showed comparable behaviour. Positive excess pore pressure generation resulted in a reduction in the vertical effective stress and gradual progression of the stress paths leftwards along the x-axis with each cycle of shear stress, towards the critical state line. During EQ3, a large reduction in vertical effective stress occurred within one cycle of shear stress, which rapidly moved the stress path leftwards toward the critical state line. Following the initial cycle, the stress path cycled at an approximately constant vertical effective stress for the remainder of shaking.

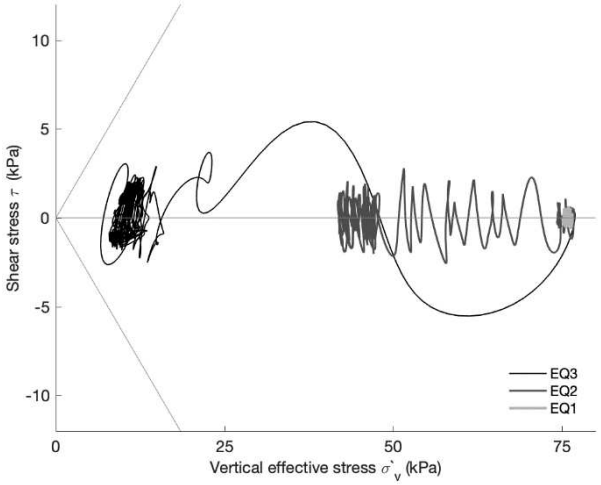

Figure 5. Stress paths at the depth of L2 of instrumentation underneath the centre of the basement. Critical state line shown.

3.4 *Settlement*

Physical modelling and numerical simulations have shown the rate of settlement of structures to be greater during the co-seismic period than in the post-seismic period (Adamidis and Madabhushi 2018, Dashti et al. 2010a, Zeybek and Madabhushi 2016). The observations from the centrifuge test presented in this paper are consistent with these observations, therefore this section will focus on displacements during the co-seismic period.

The co-seismic change in vertical displacement of the basement, which was rigidly connected to the ground floor of the superstructure is shown by the solid lines in Figure 6 alongside the vertical displacement of the soil surface adjacent to the structures shown by the dashed lines. Negative vertical displacement corresponds to settlement and positive vertical displacement corresponds to uplift.

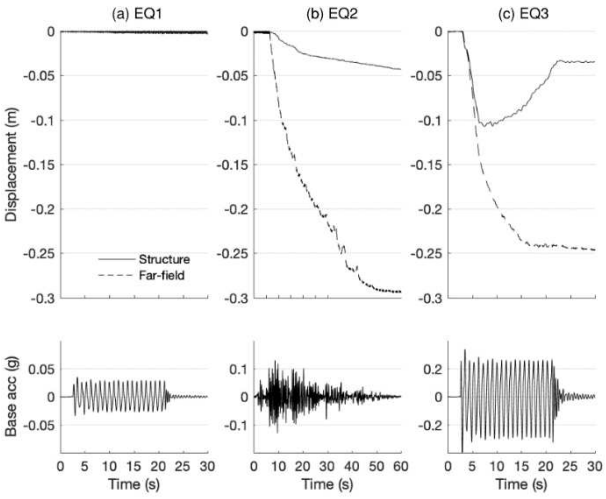

Figure 6. Co-seismic vertical displacement. Settlement is negative vertical displacement during (a) EQ1, (b) EQ2, and (c) EQ3.

During EQ1, the structure experienced negligible settlement, less than 1 mm (Figure 6a). Liquefaction occurred at shallow depths in EQ2 and resulted in the structure settling 40 mm whilst the soil adjacent to it settled 290 mm (Figure 6b). During EQ3, where liquefaction occurred in the entire column of soil beneath the basement, the structure initially settled (peak 120 mm), before uplifting (Figure 6c). The increase in excess pore pressure, shown in Figure 3c, increased the uplift force, $F_{U,L}$, acting on the

basement (see Eq. 2 and 3). This reduced the total settlement at the end of shaking to 35 mm. This is in contrast to a comparable structure without a basement which settled 430 mm during comparable base shaking (Hughes, F.E. and Madabhushi, S.P.G. 2019). The presence of a basement had the positive desired effect of notably reducing the settlement of the structure.

4 CONCLUSIONS

During small magnitude shaking events (EQ1 and EQ2), the structure with a basement presented in this paper performed advantageously. It accumulated minimal settlement, despite shaking being strong enough to cause the adjacent soil surface to settle. Horizontal accelerations were neither attenuated nor amplified as they transmitted through the saturated loose sand layer to the structure.

The large amplitude base shaking of EQ3 was sufficient to cause contraction of the loose soil skeleton, resulting in excess pore pressure generation in the soil beneath the structure. The uplift force provided by the presence of the basement increased. Consequently, the effective weight of the structure reduced. This had the positive effect of reducing liquefaction induced settlement of the structure, compared to structures with shallow foundations without a basement. In addition, generation of excess pore pressure, and the reduction in effective vertical stress that ensues, result in the stiffness of the soil approaching an almost zero value. Transmission of S_h waves therefore decrease, causing horizontal accelerations to be attenuated as they were transmitted upwards from the base of the model, resulting in natural isolation of the structure.

5 ACKNOWLEDGEMENTS

The assistance of the technicians at the Schofield Centre with running the centrifuge tests must be acknowledged. The first author would like to thank the Engineering and Physical Sciences Research Council (EPSRC) for their financial support funding the costs associated with this research project, and the British Geotechnical Association (BGA) for the financial support to attend this conference.

6 REFERENCES

Adamidis, O. and Madabhushi, S.P.G. 2018. Deformation mechanisms under shallow foundations on liquefiable layers of varying thickness. *Géotechnique* 68(7), 602–613.

Arias A (1970). A measure of earthquake intensity. Seismic Design for Nuclear Power Plants, RJ Hansen, ed., MIT Press, Cambridge, Massachusetts.

Bertalot, D. and Brennan, A.J. 2015. Influence of initial stress distribution on liquefaction-induced settlement of shallow foundations. *Géotechnique* 65(5), 418–428.

Bertalot, D., Brennan, A.J. and Villalobos, F.A. 2013. Influence of bearing pressure on liquefaction- induced settlement of shallow foundations. *Géotechnique* 63(5), 391–399.

Chian S.C., Stringer M.E. and Madabhushi S.P.G. 2010. Use of automatic sand pourers for loose sand models. *Proc. 7th Int. Conf. on Physical Modelling in Geotechnics*, Zurich, Switzerland.

Chian, S.C. and Madabhushi, S.P.G., 2012. Effect of buried depth and diameter on uplift of underground structures in liquefied soils. *Soil Dynamics and Earthquake Engineering* 41(1), 181–190.

Cubrinovski, M., Bray, J.D., Taylor, M., Giorgini, S., Bradley, B., Wotherspoon, L., and Zupan, J. 2011. Soil Liquefaction Effects in the Central Business District during the February 2011 Christchurch Earthquake. *Seismological Research Letters* 82(6), 893–904.

Dashti S., Bray J.D., Pestana J.M., Riemer M., Wilson D. 2010b. Mechanisms of Seismically Induced Settlement of Buildings with Shallow Foundations on Liquefiable Soil. *Journal of Geotechnical and Geoenvironmental Engineering* 136(1), 151–164.

Dashti, S., Bray, J.D., Pestana, J.M., Riemer, M. and Wilson, D. 2010a. Centrifuge Testing to Evaluate and Mitigate Liquefaction-Induced Building Settlement Mechanisms. *Journal of Geotechnical and Geoenvironmental Engineering* 136(7), 918–929.

Elgamal, A. W., Zeghal, M. and Parra, E. 1996. Liquefaction of reclaimed island in Kobe, Japan. *Journal of Geotechnical Engineering* 122(1), 39 – 49.

Hughes, F.E. and Madabhushi, S.P.G. 2019. Co-seismic rotation and displacement of a structure with a basement sited in liquefiable soil. *Proc. 7th Int. Conf. on Earthquake Geotechnical Engineering* 2898-2905.

Hughes, F.E. and Madabhushi, S.P.G. 2019. Liquefaction induced displacement and rotation of structures with wide basements. *Soil dynamics and earthquake engineering* 120, 75-84.

Koseki, J., Matsuo, O. and Koga, Y. 1997. Uplift behaviour of underground structures caused by liquefaction of surrounding soil during earthquake. *Soils and Foundations* 37(1), 97–108.

Mitrani H. 2006. Liquefaction Remediation Techniques for Existing Buildings. Ph.D. Thesis, University of Cambridge.

Schofield A.N. 1980. Cambridge Geotechnical Centrifuge Operations. *Géotechnique* 30(3), 227–268.

Steedman R.S. and Madabhushi S.P.G. 1991. Wave propagation in sand medium. *Proc. 4th Int. Conf. on Seismic Zonation,* Stanford, California.

Stringer M.E and Madabhushi S.P.G. 2010. Improving model quality through computer controlled saturation. *Proc. 7th Int. Conf. on Physical Modelling in Geotechnics*. Zurich, Switzerland.

Yang, D., Naesgaard, E., Byrne, P.M., Adalier, K. and Abdoun, T. 2004. Numerical Model Verification and Calibration of George Massey Tunnel using Centrifuge Models. *Canadian Geotechnical Journal* 41(5), 921–942.

Yasuda, S., Harada, K., Ishikawa, K. and Kanemaru, Y. 2012. Characteristics of liquefaction in Tokyo Bay area by the 2011 Great East Japan Earthquake. *Soils and Foundations* 52(5), 793–810.

Zeybek A and Madabhushi S.P.G. 2016. Centrifuge testing to evaluate the liquefaction response of air-injected partially saturated soils beneath shallow foundations. *Bulletin of Earthquake Engineering* 15(1), 339–356.